

RESEARCH

Open Access



# Unveiling the therapeutic potential of anthocyanin/cisplatin-loaded chitosan nanoparticles against breast and liver cancers

Mai G. Awad<sup>1</sup>, Nemany A. N. Hanafy<sup>2</sup>, Ramadan A. Ali<sup>1</sup>, Dalia D. Abd El-Monem<sup>1</sup>, Sara H. El-Shafey<sup>1</sup> and Mohammed A. El-Magd<sup>3\*</sup> 

\*Correspondence:  
mohamed.abouelmagd@vet.kfs.edu.eg

<sup>1</sup> Zoology Department, Faculty of Women for Arts Science and Education, Ain Shams University, Cairo 11757, Egypt

<sup>2</sup> Group of Bionanotechnology and Molecular Cell Biology, Institute of Nanoscience and Nanotechnology, Kafrelsheikh University, Kafrelsheikh 33516, Egypt

<sup>3</sup> Department of Anatomy, Faculty of Veterinary Medicine, Kafrelsheikh University, Kafrelsheikh 33516, Egypt

## Abstract

**Background:** Liver and breast cancers are among the leading causes of cancer-related deaths worldwide, prompting researchers to seek natural anticancer agents and reduce chemotherapy side effects. Red beetroot (*Beta vulgaris* Linnaeus), rich in polyphenols and powerful antioxidants, has shown potential in cancer prevention. This study aimed to evaluate the impact of red beetroot-derived anthocyanin (Ant), Ant-loaded chitosan nanoparticles (Ant NPs), cisplatin (Cis), Cis-loaded chitosan (Cis NPs), and Cis + Ant-loaded chitosan NPs on human hepatoma HepG2 and breast adenocarcinoma MCF7 cell lines.

**Methods:** NPs preparation was evaluated by zeta potential, FTIR, and SEM. The cytotoxic, apoptotic, antioxidant, anti-inflammatory, anti-metastatic, and anti-angiogenic effects were assessed by MTT assay, qPCR, AO/EB staining, and flow cytometry.

**Results:** Treatment with Ant, Ant NPs, Cis, Cis NPs, and Cis + Ant NPs caused cytotoxicity in HepG2 and MCF7 with best effect in Cis-treated cells. The anticancer effects were attributed to mitochondrial-dependent apoptosis (with high *Bax* and low *Bcl2* expression), chromatin disintegration, and cell cycle arrest in G2/M and S phases. All treatments inhibited migration by downregulating the migration-related gene *MMP9* and upregulating the anti-migratory gene *TIMP1* and decreased the angiogenesis-related gene *VEGF* and the inflammatory gene *TNFA* with best results in Cis NPs-treated cells. Interestingly, Ant, Ant NPs, and Cis + Ant NPs increased the antioxidant status (high GSH and upregulated expression of *Nrf2* and *OH-1*) and decreased drug resistance-related *MAPK1* and *MDR1* genes compared to Cis and Cis NPs-treated cells.

**Conclusions:** Anthocyanin and cisplatin-loaded chitosan nanoparticles effectively combat breast and liver cancers by inducing cancer cell apoptosis, enhancing antioxidant defenses, and reducing inflammation. They also inhibit tumor spread and blood vessel formation through downregulation of *MMP9* and *VEGF*, highlighting their therapeutic potential.

**Keywords:** Anthocyanin, Beetroot, Cisplatin, Nanoparticles, Anticancer, Apoptosis



## Introduction

Despite extensive research and significant investments, cancer remains a complex and challenging disease that remains elusive to comprehensive understanding and effective treatment. Among Egypt's most prevalent cancers are breast and liver cancers (Abdelkawy et al. 2020; Al-Muftah and Al-Ejeh 2023). Breast cancer is one of the most prevalent cancers globally, typically treated with surgery, radiation, chemotherapy, and hormonal therapy (Łukasiewicz et al. 2021; Siegel et al. 2020). While survival rates are relatively high for early stage breast cancer, advanced or metastatic cases still face limited treatment options and poorer outcomes, often due to drug resistance (Obidiro et al. 2023). Liver cancer, particularly hepatocellular carcinoma (HCC), is more challenging to treat, with options like surgical resection, liver transplantation, ablation, and chemotherapy offering limited success, especially in advanced stages. The prognosis for liver cancer remains poor, as it is often diagnosed at a late stage, and many patients develop resistance to current therapies like sorafenib (Attia et al. 2022; Forner et al. 2018). Unfortunately, the eradication of all cancer cells by these treatments exhibits poor effectiveness due to toxicity and resistance (He and Shi 2014). Novel approaches are urgently needed for both cancers due to treatment resistance, side effects from conventional therapies, and the need for more targeted, less toxic treatments that can improve long-term survival and quality of life for patients (Falzone et al. 2018). In recent decades, cancer treatment has advanced with the rise of targeted therapies (Anand et al. 2023; Attia et al. 2022). Breast cancer treatment has seen notable improvements in recent years, with advances in targeted therapies (such as HER2 and PARP inhibitors) improving survival rates and prognosis for many patients (Masoud and Pagès, 2017).

HepG2 cell line, derived from human hepatocellular carcinoma, demonstrates epithelial structure, exhibiting important liver-specific activities, such as generation of plasma proteins, bile acids, and drug metabolism. These cells were extensively used in liver cancer research; however, they do not possess the whole metabolic capacities of mature liver cells (Chen et al. 2021; Lv et al. 2022). MCF7 cell line, derived from human metastatic breast cancer, exhibits estrogen receptor positivity (ER+), is receptive to hormones, and well-suited for investigating breast malignancies influenced by estrogen and mechanisms of anti-cancer chemotherapy. However, it is exclusively applicable to ER+ breast cancer, therefore restricting its use to other subtypes of breast cancer (Zbiral et al. 2023). Both cell lines are crucial models for laboratory studies on liver and breast cancer, facilitating the development of drugs and enhancing our knowledge of cancer biology (Zedan et al. 2021).

Cisplatin (Cis), a platinum-based chemotherapy drug, has been used to treat various cancers, including liver and breast cancers. It works by crosslinking DNA, leading to apoptosis in rapidly dividing cells. However, its clinical use is often limited by toxicity and drug resistance (Awad et al. 2020). Cis is associated with severe side effects and toxicities, such as gastrointestinal issues like nausea, vomiting, and diarrhea, which can lead to malnutrition. It can also cause hemorrhagic complications, including gastrointestinal bleeding, and suppress the immune system, increasing the risk of infections. One of the most significant toxicities is nephrotoxicity, where Cis damages kidney cells, potentially leading to acute kidney injury and long-term renal dysfunction (Abass et al. 2024; Zraik and Heß-Busch 2021). As an attempt to mitigate these side effects, scientists

have successfully reduced the therapeutic dosage of Cis and administered it in combination with other anti-cancer drugs (Romani 2022). In addition, some researchers have transformed Cis into its nanoparticle (NP) form (Cis-encapsulated polymeric NPs) to minimize its side effects and enhance therapeutic efficacy (Jeong et al. 2018; Joshy et al. 2022).

Recently, there has been an urgent need for new drugs with novel modes of action to decrease the serious side effects of cancer chemotherapy, and thus, the exploration of naturally derivative compounds has been considered for cancer treatment (El-Magd et al. 2017; Ghaffari et al. 2021). Multiple compounds obtained from natural sources are evaluated as novel possible anticancer agents (Lin et al. 2020; Mazalovska and Kouokam 2020). These natural antioxidants, particularly polyphenols have potent anti-cancer and anti-inflammatory properties (Benchagra et al. 2021; Selim et al. 2019; Tawfic et al. 2024). Anthocyanins (Ants), phytochemicals that give plants their purple or red color, are well-known phenolic compounds with exceptional antioxidant, anti-inflammatory, and anticancer potentials (Salehi et al. 2020; Tsai et al. 2023). They have been shown to suppress the growth of HepG2 cells by inducing cell cycle arrest and promoting apoptosis (Fan et al. 2022). They also exhibit strong cytotoxicity against MCF7 breast cancer cells by inhibiting the ERK1/2 signaling pathway and reducing oxidative stress (Rabelo et al. 2023). However, Ants therapeutic uses are limited due to their instability, poor absorption, low bioavailability, and quick degradation after consumption (Shen et al. 2022). To overcome these shortcomings, scientists transformed Ants into its NP form (Gonçalves et al. 2022). Indeed, Ant extract from haskap berries encapsulated in chitosan NPs exhibited cytoprotective properties on human normal lung epithelial BEAS-2B cells and improved Ant delivery to the lungs (Amararathna et al. 2022). Some studies investigated the anticancer potential of Ant encapsulated in NPs on human erythroleukemic (Thibado et al. 2018) and melanoma cancer cells (Ghiman et al. 2021) and found potent cytotoxic effects. Moreover, combining Ants and Cis have shown synergistic effects in both HepG2 and MCF7 cells, allowing for the co-delivery of both agents, reducing the required dose, and improving their therapeutic outcomes (Yang et al. 2020; Zhang et al. 2022). However, to the best of our knowledge, the impact of Ant/Cis-loaded chitosan NPs on breast or liver cancers has not been elucidated thus far.

Based on the previous information, it becomes evident that there is a scientific deficiency in the studies that investigated the therapeutic impacts of Ant and Cis-loaded chitosan NPs together against breast and liver cancers. Therefore, we conducted this experiment to evaluate the therapeutic potential of this combination in breast and liver cancer cells.

## **Materials and methods**

### **Cell lines, chemicals, and reagents**

HepG2 and MCF7 cells were obtained from the National Cancer Institute in Cairo, Egypt. Cisplatin (CISPLATINE MYLAN, DCI #: 05G111), and ethanol were acquired from Baker Analysed (Fisher Scientific, Landsmeer). The chitosan was purchased from Fluka-Sigma Aldrich LLC (St. Louis, MO, USA). Tissue culture reagents included DMEM, trypsin, fetal bovine serum (FBS), l-glutamine, penicillin/streptomycin, dimethyl sulfoxide (DMSO), and MTT were obtained from Sigma and GIBCO (New York,

USA). The Gene JET RNA Purification Kit was purchased from Thermo Scientific, the Quantiscript Reverse Transcription Kit, and Quanti-Tect SYBR Green PCR Kit from Qiagen (Germany). Every other reagent and chemical were of the utmost purity attainable.

#### **Extraction of anthocyanin**

The red beetroot (*Beta vulgaris* L.) was purchased from a local market in Kafrelsheikh city, 0.25 kg was weighed, washed by running tap water, to remove any dust or foreign materials from its surface, cut into uniform pieces with a knife, and transported to a 1000 mL beaker. An appropriate amount of 95% ethanol was added to the beaker, which was fully covered with foil to prevent alcohol volatilization and light exposure to prevent anthocyanin (Ant) breaking. The rotation was done under heating using a stirrer magnet at 65 °C for 3 h. After the color had changed to dark red, the extract was filtrated and evaporated in an oven at 40 °C for 48 h and the filtrate was stored at 4 °C until use for NP fabrication (Hanafy 2021). The beetroot extract was examined by UV–visible spectrophotometer and FTIR. An equal volume of the beetroot extract and NaOH (1 mL: 1 mL) was heated for 10 min at 100 °C. The presence of Ant is indicated by a dark bluish-green color, while the formation of a yellow color signifies the presence of betacyanin (Parveen Zia 2021).

#### **Quantification of total anthocyanin**

The sulfur dioxide (SO<sub>2</sub>) bleaching procedure was used to assess the concentration of total Ant (Fig. S1) (Guiné et al. 2018). In this approach, a stock solution of 5 mL of beetroot extract and 5 mL of ethanol acidified with 0.1% HCl was made, and the pH was adjusted to 0.6 with 0.5% HCl. From the stock solution, two flacon tubes (15 mL) were prepared as follows: tube 1 (t1) is composed of 2 mL of the stock solution mixed with 0.8 mL of water. Tube 2 (t2) is composed of 2 mL of the stock solution mixed with 0.4 mL of HNaSO<sub>4</sub> solution (15% w/v). Following a 20-min incubation period in darkness at room temperature, the absorbance was quantified at a wavelength of 520 nm. The total Ant was estimated using the following equation: Ant (mg Mv3G/g) = 875 × [absorbance of tube 1 (abst1) – abst2], and results were shown as malvidin equivalents, based on sample mass and extract volume to obtain an absorbance between 1.500 and 2.000 (Guiné et al. 2019). The analyses were performed in triplicate for each sample.

#### **Fabrication of anthocyanin nanoparticles**

The Ant extract was dissolved in chitosan, citric acid was supplemented, the mixture was agitated for a duration of 30 min at ambient temperature, dialyzed against distilled H<sub>2</sub>O, and kept at – 20 °C for 24 h before being used for lyophilization (Hanafy et al. 2023).

#### **Fabrication of cisplatin nanoparticles**

The process involved mixing Cis with polyacrylic acid, sonicating it, adding both chitosan and citric acid, and dialyzing vs distilled H<sub>2</sub>O. The assembly was kept at – 20 °C for 24 h before transferring to the lyophilization process. The ingredients were stored at – 20 °C until used. The process was repeated to remove unreacted materials and ensure the correct mixture was prepared (Sultan et al. 2022).

### **Fabrication of cisplatin and anthocyanin nanoparticles**

Cis and polyacrylic acid were mixed, sonicated, and then Ant extract, chitosan, and citric acid were added. The mixture was dialyzed vs distilled H<sub>2</sub>O and stored at – 20 °C for 24 h before transferring to the lyophilization process. The ingredients were then stored at – 20 °C until needed.

### **Construction of standard curve for calculating encapsulated cisplatin concentration**

The linearity of Cis was determined by drawing a calibration curve to determine Cis NPs concentration. Cis NPs were centrifuged (10,000 rpm/30 min) and the supernatant was measured at 301 nm. The supernatant was utilized to determine Cis loading capacity through a UV–visible spectrophotometer. The slope, intercept, and  $R^2$  values for Cis were 0.1235, 0.0002, and 0.999, respectively. Cis calibration curve ( $y=0.1235x-0.0002$ ;  $R^2=0.999$ ) in 5 mg/mL distilled water was prepared with a Cis concentration range of 312.5 to 5000 µg/mL.

### **Determination of loading capacity and encapsulation efficiency (EE)**

For Cis, we used this equation:  $EE (\%) = (\text{Cis total concentration} - \text{free Cis concentration (supernatant)}) / \text{Cis total concentration} \times 100$ . The concentration of Cis in the capsule was calculated after calculating the specific EE of Cis. For Ant, we utilized this equation:  $EE (\%) = (\text{Ant total amount (mg)} - \text{Ant amount in the supernatant}) / \text{Ant total amount} \times 100$  (Venancio et al. 2017). Ant concentration inside the capsule was determined by calculating the total Ant in the extract and supernatant produced after centrifugation of the Ant NPs. The Ant total amount and the amount in the supernatant after encapsulation were calculated by using SO<sub>2</sub> bleaching.

### **Characterization of Ant, Cis and their NPs**

To characterize the shape of the synthesized NPs, we used scanning electron microscopy (SEM) using 5 kV-accelerating potential electron beams (JEOL, JSM-IT 100) and SEM/JSM 5000 program. To detect surface molecule structures, we utilized the Fourier Transform Infrared Spectrometer (FTIR, JASCO, JAPAN, model no. AUP1200343) in the 500–4000 cm<sup>1</sup> range using the KBr pellet method. At least three scans were performed on various parts of the samples, and representative spectra were analyzed. We also measured the absorbance of samples at wavelengths between 200 and 800 nm using a Shimadzu UV–visible spectrophotometer (UV-1800, Shimadzu Corporation, Japan). Photon correlation spectroscopy was used to determine the electrophoretic mobility of samples using a Zeta Nano Sizer (Zetasizer Nano ZS, Malvern Panalytical, United Kingdom), and data were collected at room temperature (approximately 25 °C).

### **Cell culture**

The frozen HepG2 and MCF7 cell lines were thawed, transferred to a sterile falcon containing DMEM, and centrifuged. The cell pellet was suspended in the culture medium and cultured at 37 °C for 3 days under 5% CO<sub>2</sub>, and 95% air. Culture renewal was done at 80–90% confluence for 5 days and the cells were then cultured at the desired dilution in new flasks.

### Cell viability by MTT assay

The MTT assay is based on the ability of metabolically active cells to reduce yellow tetrazolium salt into purple formazan crystals. This reduction occurs in the mitochondria of living cells, and the amount of formazan produced is directly proportional to the number of viable cells (Ghasemi et al. 2023). In a complete media [DMEM, 10% FBS, and 1% antibiotic (GIBCO, New York, USA)], cells (10,000 cells/well) were cultured (37 °C, 5% CO<sub>2</sub>) for 24 h. After reaching 70–80% confluence, cells were treated with Cis, Ant, Cis NPs, Ant NPs, and Cis + Ant NPs at doses of 0, 3.125, 6.25, 12.5, 25, 50, and 100 µg/mL and incubated for 1 day. Following the addition of 20 µL of MTT solution (5 mg/mL), the cells were incubated for a further 4 h. Following formazan crystal dissolution in 100 µL DMSO, absorbance was measured at 570 nm. The IC<sub>50</sub> was determined from the sigmoidal dose–response curve generated using GraphPad Prism. Percent cell viability was calculated using the following formula: cell viability (%) = [(OD of treated cells – OD of blank) / (OD of control cells – OD of blank)] × 100. Control (untreated) cells were considered 100% viable, and the percent viability of treated cells was calculated relative to the control. Each experiment was performed in triplicate to ensure reproducibility.

### Acridine orange and ethidium bromide double staining

Acridine orange (AO) and ethidium bromide (EB) double staining is a fluorescence-based method used to differentiate live, apoptotic, and necrotic cells. AO is a cell-permeable dye that stains both live and dead cells, emitting green fluorescence when bound to double-stranded DNA in viable cells. EB is only permeable to dead cells with compromised membranes and binds to DNA, emitting red fluorescence. The combination allows for distinguishing viable cells (green), early apoptotic cells (yellow-green with condensed or fragmented chromatin), and necrotic or late apoptotic cells (red) (Kari et al. 2022). Cells were typically seeded at a density of  $1 \times 10^5$  cells/mL into a 6-well plate or 24-well plate. This ensures sufficient cell number for microscopic examination. Following treatment of cancer cells with Cis, Ant, and NPs of Cis or/and Ant at concentrations equal to their IC<sub>50</sub> for 24 h, the cells were fixed with 4% paraformaldehyde, stained with 10 µL of 1 mg/mL AO and EB mixture per well (double staining approach), and images were captured using fluorescence microscopy (Nikon's Eclipse Ti2, Japan) at 20× magnification.

### Gene expression analysis by qPCR

Quantitative PCR (qPCR) was used to quantify gene expression levels. Total RNA was isolated from MCF7 and HepG2 cells using a commercially available RNA isolation kit, the RNA concentration and purity were measured using a spectrophotometer. RNA was reverse transcribed into complementary DNA (cDNA) using a reverse transcription kit. A reaction mix was prepared that included the cDNA template, gene-specific primers (Table S1), a fluorescent dye SYBR Green Kit. The qPCR thermal cycling conditions included initial denaturation at 95 °C (for 10 min), followed by 40 cycles of denaturation at 95 °C (for 15 s) and annealing/extension at 60 °C (for 40 s). Gene expression levels were quantified using the  $2^{-\Delta\Delta C_t}$  method. A stable housekeeping *GAPDH* gene was used as an internal control to normalize the expression levels of the target gene. The fold change was calculated relative to the control group. A fold change > 1 indicates

upregulation, while a fold change  $< 1$  indicates downregulation of the gene in the treated sample compared to the control (Attia et al. 2022; Selim et al. 2019).

#### Detection of the cell cycle by flow cytometry

HepG2 and MCF7 were seeded in 6-well plates at a density of  $1 \times 10^5$  cells per well, ensuring adequate cell growth before treatment. The cells were treated with  $IC_{50}$  value of Cis, Ant extract, and/or their NPs. After 24 h treatment, cells were trypsinized using 0.25% trypsin–EDTA, collected, and centrifuged at 500 rpm for 5 min. Cells were then washed twice with cold PBS to remove excess media. Cells were fixed by resuspending them in 70% ice-cold ethanol and incubating for 24 h at  $-20$  °C. This step preserves the cells and permeabilizes the membrane, allowing propidium iodide (PI) to enter. After fixation, cells were washed twice with PBS to remove ethanol. Cells were resuspended in 500  $\mu$ L of PI staining solution, which contains; 50  $\mu$ g/mL PI for DNA staining, 100  $\mu$ g/mL RNase A (to degrade RNA and ensure that only DNA is stained), and 0.1% Triton X-100 to help permeabilize the cells. The cells were incubated in the PI staining solution at 37 °C for 30–60 min in the dark to allow proper staining of nuclear DNA. After incubation, the cells were ready for analysis using FACScan (BD Biosciences, One Becton Drive Franklin Lakes, NJ, USA) and FlowJo V.10 (BD Biosciences). About 10,000 events were collected per sample to ensure statistical relevance for cell cycle analysis.

#### Evaluation of reduced glutathione (GSH)

Cells were collected after 24 h of treatment and the levels of GSH were determined calorimetrically using a commercial kit (Bio-Diagnostics Co, Egypt) according to the manufacturer's instructions. The results are expressed as a percentage of the control, with the control level set at 100%.

#### Statistical analysis

The statistical method applied in our study was one-way ANOVA followed by Tukey's post hoc test to identify whether differences between treatments were significant ( $P < 0.05$ ) or not ( $P > 0.05$ ). Data were expressed as mean  $\pm$  SEM. Graph Pad Prism 8 software was used in statistical analysis.

## Results

#### Characterization of Ant, Cis, and their NPs

Ant spectra mainly depend on pH and their absorbance values were evaluated at the peak wavelength of 512 nm (Stavenga et al. 2020). SEM examination revealed that Ant NPs are spherical and were separately distributed (Fig. S2A). The UV–visible spectrophotometer of Ant displayed three peaks at 265, 482, and 539 nm (Fig. 1A), and Ant NPs showed three peaks at 267, 478, and 540 nm (Fig. 1A, Fig. S2B). After heating the mixture of 1 mL of the Ant and 1 mL of NaOH for 5 min at 100 °C, the resulting bluish-green color indicates the presence of Ant (Fig. S2C–E) as mentioned by Parveen Zia (2021). The UV–visible spectrophotometer for the free Cis obtained a peak around 301 nm, while in Cis NPs no real peak appeared (Fig. 1B). On the other hand, Cis + Ant NPs showed peaks at 268, 468, and 538 nm (Fig. 1C).

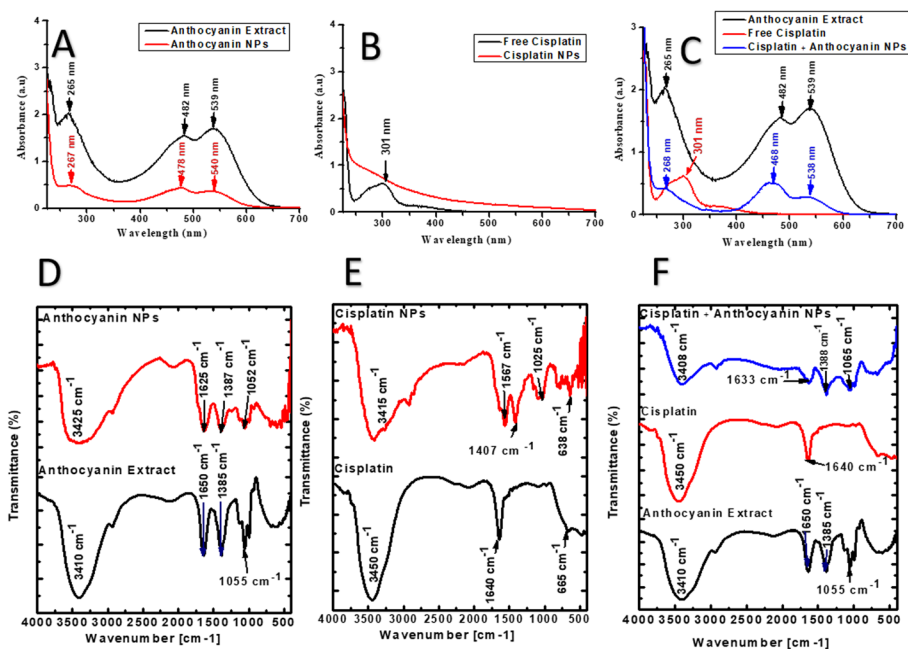


**Fig. 1** Characterization of Ant, Cis, and their NPs by UV-Vis absorption and FT-IR spectra. **A** UV-Vis absorption spectra of Ant extract and Ant NPs. **B** UV-Vis absorption spectra of Cis and free Cis NPs. **C** UV-Vis. UV-Vis absorption spectra of the Ant extract, free Cis, and Ant + Cis NPs. **D** FT-IR spectra of the Ant extract and Ant NPs. **E** FT-IR spectra of Cis and Cis NPs. **F** FT-IR spectra of the Ant extract, Cis and Ant + Cis NPs

The FT-IR spectrum of Ant and Ant NPs was recorded between  $4000\text{ cm}^{-1}$  and  $400\text{ cm}^{-1}$  at  $0.1\text{ cm}^{-1}$  resolution (Fig. 1D). The results agreed with previously reported work (Sivanukkalai Jeyaram 2020). The intense broadband at  $3410\text{ cm}^{-1}$  in the FT-IR spectrum of Ant was assigned to  $-\text{OH}$  stretching vibrations which also appeared in Ant NPs at  $3425\text{ cm}^{-1}$ . The aliphatic  $\text{C}-\text{H}$  stretching bands occurred between  $2900\text{ cm}^{-1}$  and  $3000\text{ cm}^{-1}$  in Ant and Ant NPs FT-IR. While the  $\text{C}=\text{N}$  stretching band appeared in Ant and Ant NPs at  $1650\text{ cm}^{-1}$  and  $1625\text{ cm}^{-1}$ , respectively. The bands at  $1385\text{ cm}^{-1}$  and  $1387\text{ cm}^{-1}$  were attributed to the bending of  $-\text{OH}$  groups. The last weak band at  $1055\text{ cm}^{-1}$  and  $1052\text{ cm}^{-1}$  was attributed to  $\text{C}-\text{H}$  bending (Jeyaram and Geethakrishnan 2020). FTIR results showed Cis preserved its chemical structure in NPs (Fig. 1E). Platinum and ammonium bonds appeared at  $665\text{ cm}^{-1}$  and  $638\text{ cm}^{-1}$  in Cis and Cis NPs, respectively. In addition to the presence of tensional trembles of ammonium groups that emerged in  $3450\text{ cm}^{-1}$  (Cis) and  $3415\text{ cm}^{-1}$  (Cis NPs) (Babaei et al. 2019). In a spectrum of Cis + Ant NPs, stretching vibrations of  $-\text{OH}$  appeared at  $3408\text{ cm}^{-1}$ . While the band located at  $1633\text{ cm}^{-1}$  revealed the presence of Cis, and the band that appeared at  $1388\text{ cm}^{-1}$  indicated the presence of Ant (Fig. 1F).

The dynamic light scatters (DLS) detected mean zeta potential values of Ant NPs, Cis NPs, and Cis + Ant NPs were 50.41, 51.4, and 41.2 mV, respectively (Fig. 2A–C). DLS of the Zeta sizer indicated that the mean diameter of the Ant NPs (Fig. 2D), Cis NPs (Fig. 2E), and Cis + Ant NPs (Fig. 2F) was 183.5 nm, 143.5 nm, and 154.7 nm, respectively.

Cis NPs were prepared via ion-complex formation between carboxylic acid of poly acrylic acid (PAA) copolymer and Cis (Fig. S2F). Cis was added to an aqueous

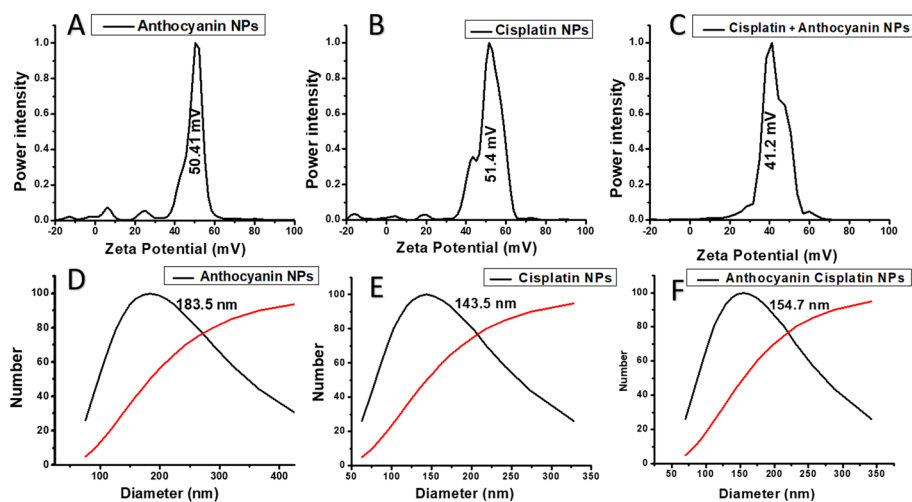


**Fig. 2** Characterization of Ant, Cis, and their NPs using Zeta potential and DLS. **A** Zeta potential of Ant NPs. **B** Zeta potential of Cis NPs. **C** Zeta potential of Ant + Cis NPs. **D** DLS of the Zeta sizer of Ant NPs. **E** DLS of the Zeta sizer of Cis NPs. **F** DLS of the Zeta sizer of Ant + Cis NPs

solution of PAA copolymer and stirred until a transparent aqueous solution was obtained. This means no aggregation appeared during the interaction of PAA and Cis. After sonication of PAA–Cis mixture, a mixture of chitosan, Ant extract, and citric acid was added with further stirring and sonication. The mixture underwent dialysis for 24 h to remove impurities, and the final product was lyophilized for 5 days, yielding stable Cis + Ant NPs (Fig. S3).

#### Determination of encapsulation efficiency and concentration of Cis and Ant inside capsules

The concentration of free Cis (in the supernatant) was 0.01097 mg/mL as calculated from this equation: Cis concentration (mg/mL) = (slope × absorbance) + intercept, where the absorbance of the supernatant at 301 nm was 0.092. The encapsulation efficiency (EE) of Cis was 99.63% based on this equation  $EE (\%) = (\text{Cis total concentration} - \text{free Cis concentration (supernatant)}) / \text{Cis total concentration} \times 100$  (Fig. 3A–C). The concentration of Cis in the capsule was estimated to be 0.10 mg/mL as we used a total of 6 mg Cis in a total volume of 60 mL and EE of Cis was 99%.

The total Ant in the extract was 103.25 mg per 100 g of fresh weight of red beetroot using a 27.900 molar extinction coefficient as calculated from this equation:  $\text{Ant (mg Mv3G/g)} = 875 \times (\text{abst1} - \text{abst2})$ , where abst1 equals 1.8 and abst2 equals 1.692. In the supernatant, the Ant amount was 39.375 mg as abst1 equals 0.16 and abst2 equals 0.115. The amount of encapsulated Ant equals 63.875 mg as estimated by subtracting the amount of the total Ant in the supernatant from the extract (Fig. 3D, E). The percentage encapsulation for Ant NPs was calculated using the following formula:  $\text{encapsulation efficiency (\%)} = (\text{encapsulated Ant} / \text{total Ant in the extract}) \times 100$ , where encapsulated Ant = 63.875 mg and total Ant in the extract = 103.25 mg. So,  $\text{encapsulation efficiency} = (63.875 / 103.25) \times 100 = 61.87\%$ .

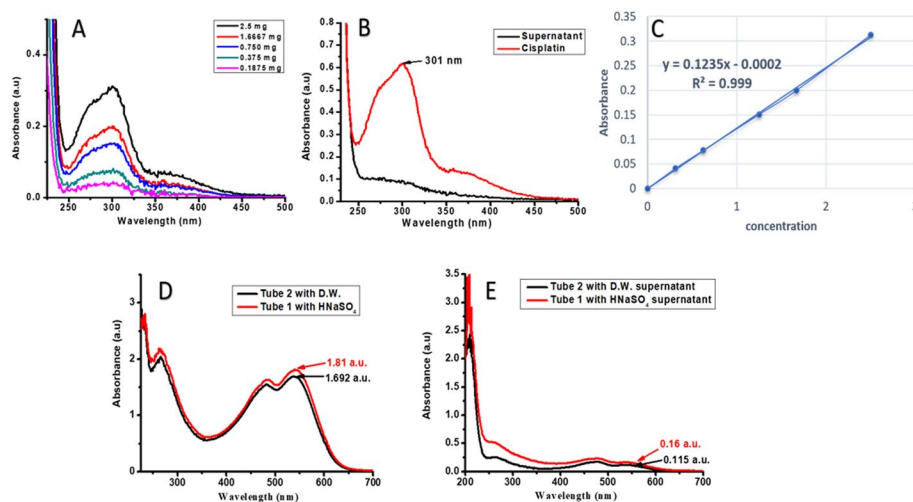


**Fig. 3** Determination of encapsulation efficiency and concentration of Cis and Ant inside capsules. **A** UV-Vis. Absorption spectra of the different Cis concentrations ranging from 312.5 to 5000  $\mu\text{g/mL}$ . **B** UV-Vis. Absorption spectra of pure Cis and the supernatant of Cis NPs after centrifugation. **C** Standard curve of Cis. **D** UV-Vis. Absorption spectra of the Ant with distilled water (D.W.) vs Ant with  $\text{HNaSO}_4$ , in the extract. **E** UV-Vis. Absorption spectra of the supernatant of Ant NPs after centrifugation

### Effect of treatments on the viability of MCF7 and HepG2 cells

MTT assay results revealed that Ant had less cytotoxic effects on MCF7 and HepG2 with  $\text{IC}_{50}$  values of  $7.17 \pm 0.86$  and  $32.62 \pm 1.51$   $\mu\text{g/mL}$ , respectively, than Cis with lower  $\text{IC}_{50}$  values of  $4.08 \pm 0.61$  and  $2.52 \pm 0.40$   $\mu\text{g/mL}$ , respectively (Fig. 4, Fig. S4). However, the Ant NPs showed higher  $\text{IC}_{50}$  values of  $57.12 \pm 1.76$  and  $61.21 \pm 1.79$   $\mu\text{g/mL}$ , and the Cis NPs showed  $\text{IC}_{50}$  values of  $21.26 \pm 1.33$  and  $18.18 \pm 1.26$   $\mu\text{g/mL}$  on MCF7 and HepG2, respectively. Encapsulation of Ant and Cis into one capsule (Cis + Ant NPs) resulted in  $\text{IC}_{50}$  values of  $20.59 \pm 1.31$  and  $33.30 \pm 1.52$   $\mu\text{g/mL}$  on MCF7 and HepG2, respectively. Conversely, when treated with empty NPs, MCF7 and HepG2 cells showed very high  $\text{IC}_{50}$  values of  $316.8 \pm 5.80$  and  $372.5 \pm 6.49$   $\mu\text{g/mL}$  on MCF7 and HepG2, respectively (Fig. 4, Fig. S4). Comparing the  $\text{IC}_{50}$  values of all treated groups in MCF7 and HepG2 cells, we found significantly decreased cytotoxicity when each drug was delivered in NP form (Fig. S5). The combined nanoparticle formulation (Cis + Ant NPs) exhibited significantly greater cytotoxic effects compared to individual nanoparticle treatments in HepG2 cells and demonstrated higher cytotoxicity than Ant NPs alone in MCF7 cells (Fig. S5).

### Ant, Cis, and their NPs induced apoptosis in MCF7 and HepG2 cells

The morphological changes (chromatin condensation or disintegration) and orange-colored nuclei of MCF7 and HepG2 stained with AO/EB revealed the potential of Ant, Cis, and their NPs to trigger apoptosis in cancer cells compared to the viable control cells which have a normal green nucleus (Fig. 5A). This apoptotic effect was confirmed on a molecular basis (in the treated cells with Ant, Ant NPs, Cis, Cis NPs, and Cis + Ant NPs) as evidenced by significant overexpression of *Bax* ( $1.64 \pm 0.19$ ,  $3.01 \pm 0.21$ ,  $3.51 \pm 0.08$ ,  $5.90 \pm 0.16$ , and  $7.84 \pm 0.28$  fold change, respectively, in MCF7 and  $1.92 \pm 0.06$ ,  $2.30 \pm 0.07$ ,  $3.10 \pm 0.04$ ,  $3.46 \pm 0.04$ , and  $4.82 \pm 0.06$  fold change, respectively, in HepG2),

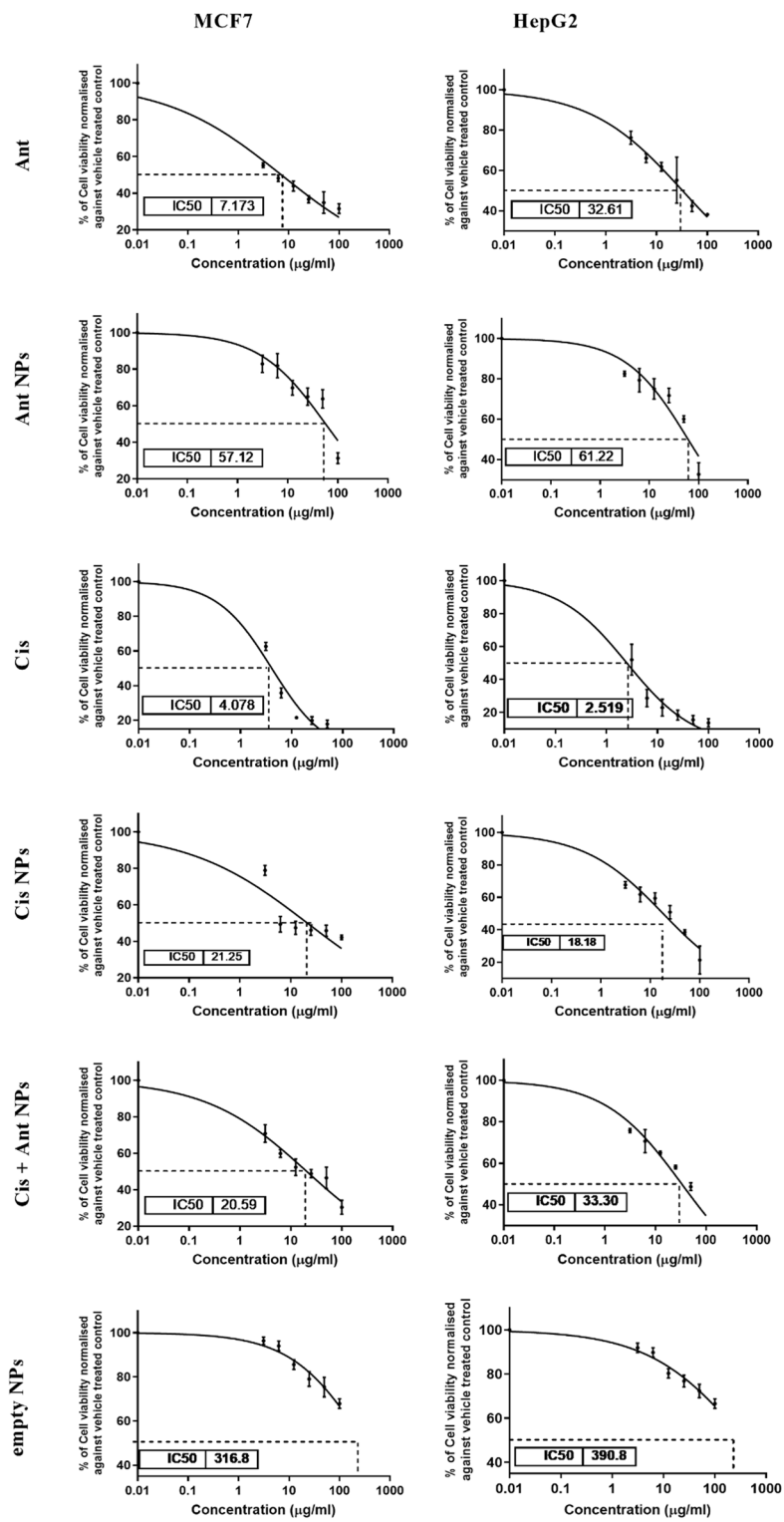


**Fig. 4** Sigmoidal curve for MTT assay displays IC<sub>50</sub> values and the inhibition % of Cis, Cis NPs, Ant extract, Ant NPs, Cis + Ant NPs, and empty NPs on MCF7 and HepG2 cells. Each data point shows an average of three independent experiments ( $n=3$ ). Data were presented as mean  $\pm$  SEM

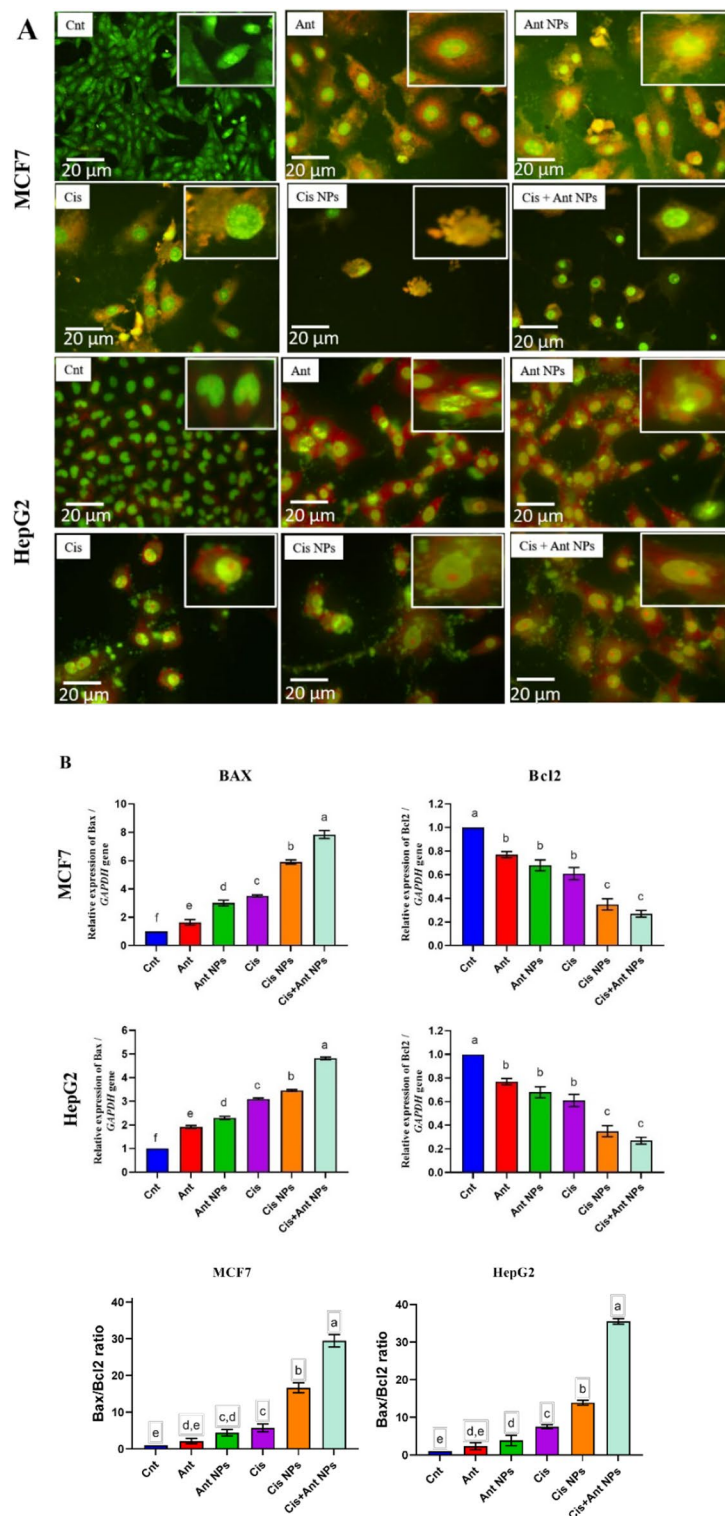


**Fig. 5** Ant, Cis, and their NPs triggered apoptosis in HepG2 and MCF7 cells. **A** Fluorescence microscopy displays the morphology of HepG2 and MCF7 stained with acridine orange/ ethidium bromide. Insets represent higher magnification of some selected cells. Scale bars = 20 μm, control (Cnt). **B** qPCR results show differential expression of the apoptotic gene *Bax*, the anti-apoptotic gene *Bcl2*, and their ratio (*Bax/Bcl2*) in MCF7 and HepG2 cells. Values are given as mean ± SEM (n = 3/group). Various letters [a (highest value)–f (lowest value)] denote significant differences at P < 0.05. All groups were compared to each other

higher *Bax/Bcl2* ratio and significant down-expression of the *Bcl2* gene ( $0.77 \pm 0.03$ ,  $0.68 \pm 0.05$ ,  $0.61 \pm 0.05$ ,  $0.35 \pm 0.05$ , and  $0.27 \pm 0.03$  fold change, respectively, in MCF7 and  $0.82 \pm 0.06$ ,  $0.60 \pm 0.05$ ,  $0.41 \pm 0.07$ ,  $0.25 \pm 0.03$ , and  $0.14 \pm 0.02$  fold change, respectively, in HepG2) relative to the control (Fig. 5B). The Cis + Ant NPs exhibited the highest apoptosis (as indicated by highest *Bax*, *Bax/Bcl2* ratio, and lowest *Bcl2* expression) followed by Cis NPs, Cis, Ant NPs, and Ant.

#### Effect of treatments on the cell cycle of cancer cells

Data obtained from flow cytometry indicated a cell cycle arrest in the G2/M phase of MCF7 and HepG2 cells as indicated by a significantly higher percentage of cells in this phase following treatment of MCF7 with Ant, Ant NPs, Cis, Cis NPs, and Cis + Ant NPs ( $15.5 \pm 0.61$ ,  $17.5 \pm 1.00$ ,  $12.32 \pm 0.83$ ,  $12.24 \pm 0.53$ , and  $15.80 \pm 0.90\%$ , respectively) and HepG2 with Ant, Ant NPs, Cis NPs ( $29.84 \pm 1.12$ ,  $27.50 \pm 1.31$ , and  $39.42 \pm 1.72\%$ , respectively), than the control ( $2.02 \pm 0.06\%$  in MCF7 and  $17.7 \pm 0.80\%$  in HepG2) (Fig. 6). In contrast, no significant results observed in HepG2 treated with Cis and Cis + Ant NPs ( $7.11 \pm 0.70$  and  $12.93 \pm 1.07\%$ , respectively). Another cell cycle arrest was noticed in the S phase of the two cells except in HepG2 cells treated with Cis and Cis + Ant NPs. Cells accumulated in the Sub G0/G1 phase revealed apoptosis. As shown in Fig. 6, all treatments induced apoptosis (as indicated by cell number in the subG0/G1 phase) in MCF7 cells, while only Cis and Cis + Ant NPs triggered apoptosis in HepG2 cells (Fig. 6).

#### Effect of treatments on the expression of drug-resistance-, metastasis-, angiogenesis-, and inflammation-related genes

To determine whether Ant, Cis and their NPs can affect the expression of drug-resistance-related genes *MAPK1* and *MDR1* (Emran et al. 2022), qPCR was applied on cDNA prepared from RNA isolated from MCF7 and HepG2. Interestingly, Cis-treated MCF7 and HepG2 cells displayed the highest significant expression of *MDR1* ( $1.41 \pm 0.09$  and  $1.54 \pm 0.037$ -fold change, respectively) and *MAPK1* ( $1.45 \pm 0.08$ , and  $1.80 \pm 0.06$ -fold change, respectively) even more than the control group. On the other hand, Ant, Ant NPs, and Cis + Ant NPs treated cells showed significantly reduced expression of *MDR1* ( $0.23 \pm 0.02$ ,  $0.07 \pm 0.01$ , and  $0.32 \pm 0.02$ -fold change in MCF7, and  $0.70 \pm 0.04$ ,  $0.44 \pm 0.03$ , and  $0.36 \pm 0.03$ -fold change in HepG2, respectively) and *MAPK1* ( $0.55 \pm 0.06$ ,  $0.39 \pm 0.03$ , and  $0.25 \pm 0.02$ -fold change in MCF7 and  $0.72 \pm 0.03$ ,  $0.54 \pm 0.04$ , and  $0.32 \pm 0.03$ -fold change in HepG2, respectively) compared to the Cis and control groups (Fig. 7).

Treatments with Ant, Ant NPs, Cis, Cis NPs, and Cis + Ant NPs also inhibited MCF7 and HepG2 migration and metastasis as indicated by significant downregulation of the metastasis-related gene *MMP9* ( $0.55 \pm 0.06$ ,  $0.27 \pm 0.02$ ,  $0.61 \pm 0.06$ ,  $0.35 \pm 0.03$ , and  $0.20 \pm 0.01$ -fold change in MCF7 and  $0.55 \pm 0.06$ ,  $0.38 \pm 0.03$ ,  $0.90 \pm 0.06$ ,  $0.41 \pm 0.05$ , and  $0.16 \pm 0.02$ -fold change in HepG2, respectively) and significant upregulation of the anti-metastatic gene *TIMP1* ( $4.63 \pm 0.06$ ,  $8.63 \pm 0.06$ ,  $3.18 \pm 0.04$ ,  $10.41 \pm 0.07$ , and  $12.47 \pm 0.06$ -fold change in MCF7 and fold change, and  $8.82 \pm 0.07$ ,  $7.94 \pm 0.06$ ,  $3.48 \pm 0.09$ ,  $5.17 \pm 0.06$ , and  $14.42 \pm 0.05$ -fold change in HepG2, respectively) compared to the control cells (Fig. 7).

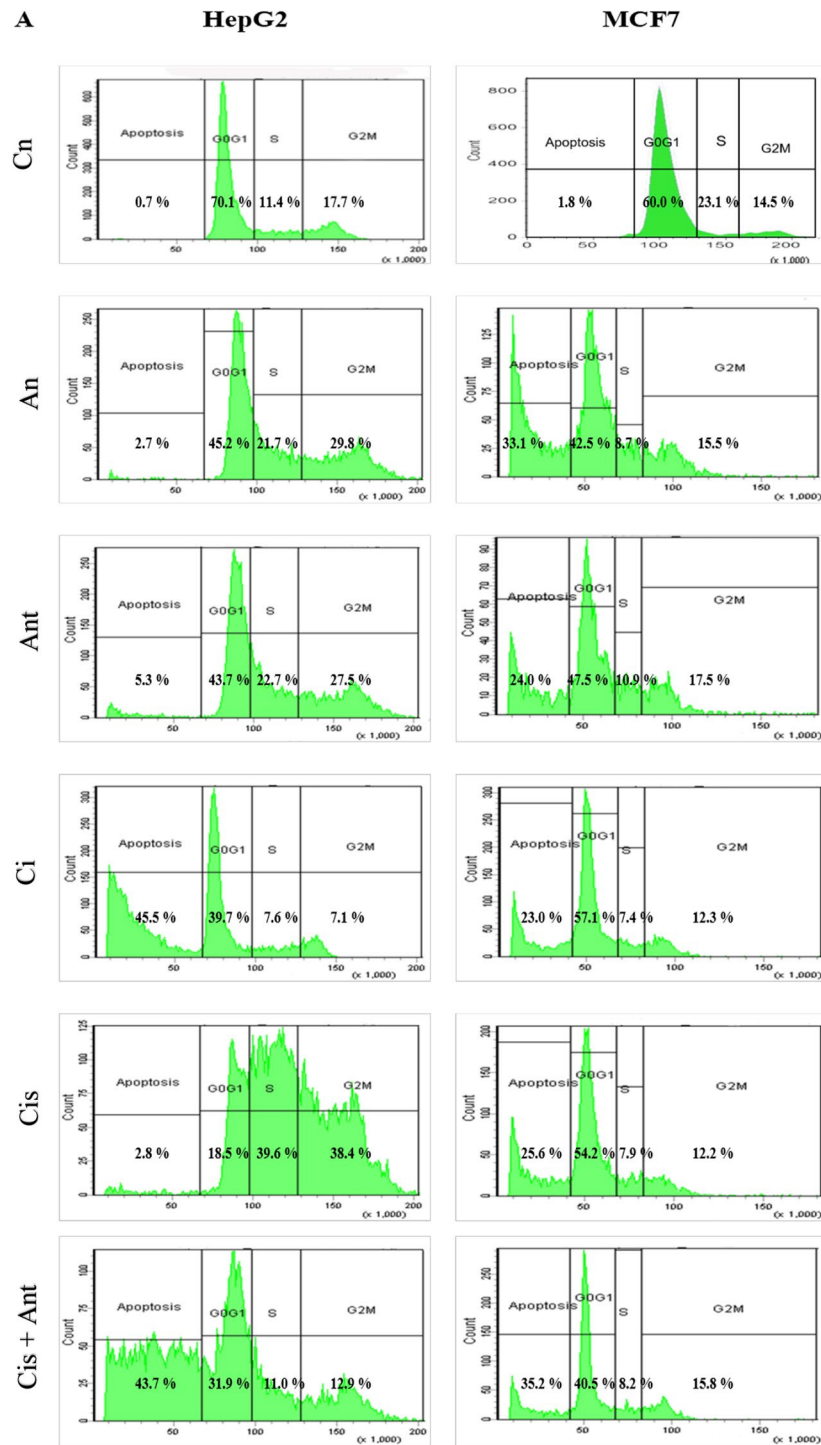


**Fig. 6** Effect of treatments on cell cycle of MCF7 and HepG2 cells. **A** Cell cycle graphs as evaluated by flow cytometry (X-axis: PI fluorescence reflecting DNA content, and Y-axis: cell count). **B** Percentage of cells in subG0/G1, G0/G1, S, and G2/M phase. Values are expressed as mean  $\pm$  SEM,  $n = 3$ . Various letters [a (highest value)–f (lowest value)] denote significant differences at  $P < 0.05$ . All groups were compared to each other

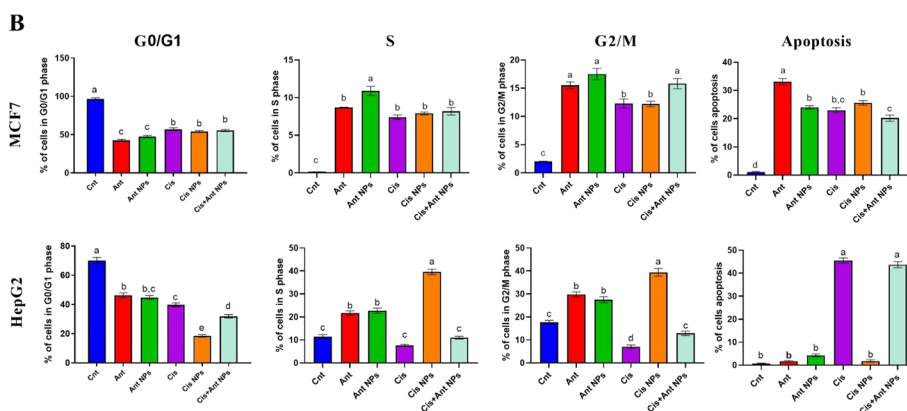
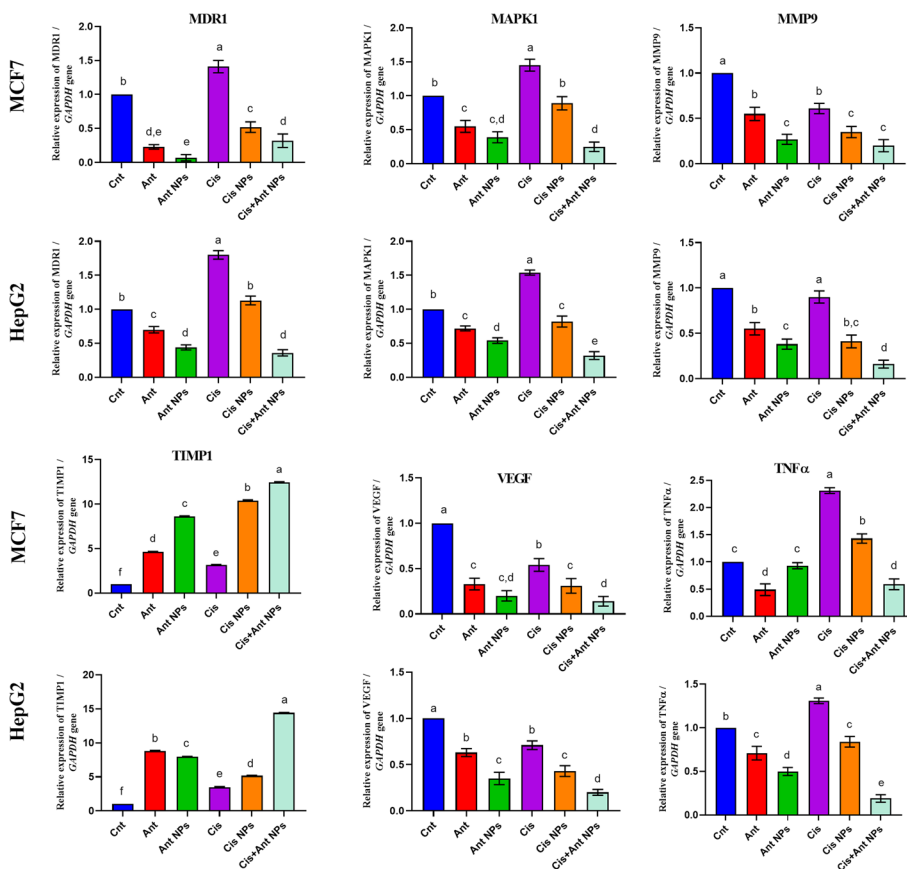


Fig. 6 continued



**Fig. 7** Real-time quantitative PCR analysis of the gene expression in MCF7 and HepG2 cells. Fold changes was calculated for *MAPK1*, *MDR1*, *MMP9*, *TIMP1*, *Nrf2*, *HO-1*, *VEGF*, and *TNFα* genes. Values are given as mean  $\pm$  SEM ( $n = 3$ /group). Various letters [a (highest value)–f (lowest value)] denote significant differences at  $P < 0.05$ . All groups were compared to each other

The expression levels of angiogenesis-related gene (*VEGF*) in MCF7 and HepG2 cell lines were significantly down-regulated in cells-treated with Ant, Ant NPs, Cis, Cis NPs, and Cis + Ant NPs ( $0.33 \pm 0.02$ ,  $0.20 \pm 0.01$ ,  $0.54 \pm 0.04$ ,  $0.31 \pm 0.02$ , and  $0.14 \pm 0.01$ -fold

change, in MCF7 and  $0.63 \pm 0.04$ ,  $0.35 \pm 0.03$ ,  $0.71 \pm 0.05$ ,  $0.43 \pm 0.05$ , and  $0.20 \pm 0.01$ -fold change, in HepG2, respectively) relative to the control cells (Fig. 7). However, the inflammation-related gene (*TNF $\alpha$* ) was significantly higher in Cis-treated cells ( $2.31 \pm 0.05$ -fold change in MCF7 and  $1.31 \pm 0.03$ -fold change in HepG2) compared to all other groups. These elevated expression levels were significantly decreased in HepG2 cells treated with Ant, Ant NPs, Cis NPs, and Cis + Ant NPs ( $0.71 \pm 0.03$ ,  $0.50 \pm 0.02$ ,  $0.84 \pm 0.06$ , and  $0.19 \pm 0.01$ -fold change, respectively) and in MCF7 cells treated with Ant, Ant NPs, and Cis + Ant NPs ( $0.49 \pm 0.02$ ,  $0.93 \pm 0.05$ , and  $0.59 \pm 0.05$ -fold change, respectively) (Fig. 7).

#### Effect of treatments on the antioxidant status

It is well-known that the anti-cancer potential of Cis is accompanied by high oxidative stress and low antioxidant activities. In parallel, we also found significantly reduced levels of GSH and expression of antioxidant-related genes (*Nfr2* and *HO-1*) in cells treated with Cis ( $69 \pm 2.3\%$ ,  $0.25 \pm 0.02$ , and  $0.06 \pm 0.01$  fold change in MCF7 and  $53 \pm 2.5\%$ ,  $0.48 \pm 0.04$ , and  $0.36 \pm 0.04$  fold change in HepG2, respectively) and Cis NPs ( $82 \pm 2.7\%$ ,  $0.06 \pm 0.01$ ,  $0.16 \pm 0.01$  fold change in MCF7 and  $0.69 \pm 0.06$ , and  $0.52 \pm 0.04$  fold change in HepG2, respectively), compared to the other groups (Fig. 8). Interestingly, Ant, Ant NPs and Cis + Ant NPs all significantly increased GSH levels ( $127.00 \pm 5.17$ ,  $132.62 \pm 5.58$ , and  $118.09 \pm 3.66\%$  in MCF7 and  $116.50 \pm 4.66$ ,  $125.77 \pm 3.93$ ,  $111.29 \pm 3.41\%$  in HepG2, respectively), *Nfr2* expression ( $3.81 \pm 0.05$ ,  $5.74 \pm 0.07$ , and  $2.43 \pm 0.05$  fold change in MCF7 and  $2.58 \pm 0.07$ ,  $3.41 \pm 0.06$ , and  $3.94 \pm 0.09$  fold change in HepG2, respectively), and *HO-1* expression ( $2.89 \pm 0.06$ ,  $3.36 \pm 0.079$ , and  $1.34 \pm 0.08$  fold change in MCF7 and  $1.69 \pm 0.07$ ,  $2.07 \pm 0.05$ , and  $2.17 \pm 0.08$  fold change, in HepG2, respectively), when compared to other groups (Fig. 8).

#### Discussion

Cis is a standard chemotherapy when used alone or in combination with other anti-cancer drugs (Romani 2022). Cis is indeed used in the treatment of several cancers, but its use in breast cancer is more limited and not typically considered a first-line treatment in many countries, including the UK (Hamaya et al. 2023). First-line treatments for breast cancer generally include hormonal therapies, targeted therapies (like trastuzumab for HER2-positive cancers), and anthracycline or taxane-based chemotherapy. However, Cis may be used in triple-negative breast cancer as platinum-based drugs have shown efficacy in these subtypes due to their DNA-damaging mechanism (Dasari and Tchounwou 2014; Elserafi et al. 2018). Cis is used more commonly in treating liver cancer, though often in specific procedures such as trans-arterial chemoembolization (TACE) which involves the localized delivery of Cis directly to the tumor through the hepatic artery, followed by embolization to block blood flow to the cancer (Aramaki et al. 2021). The benefits of Cis treatment must be weighed against the risk of severe side effects. In a recent development, Cis nanoparticles (NPs) were created to address the limitations of the drug, aiming to reduce severe side effects, low selectivity for cancer cells and improve treatment effectiveness (Jeong et al. 2018; Joshy et al. 2022). NPs can target tumors more effectively and reduce the off-target effects that lead to toxicity, such as nephrotoxicity, which is a significant issue with Cis, ototoxicity (hearing loss), neurotoxicity, and gastrointestinal disturbances (Ali et al. 2022; Duan et al. 2016). In addition, it often leads to

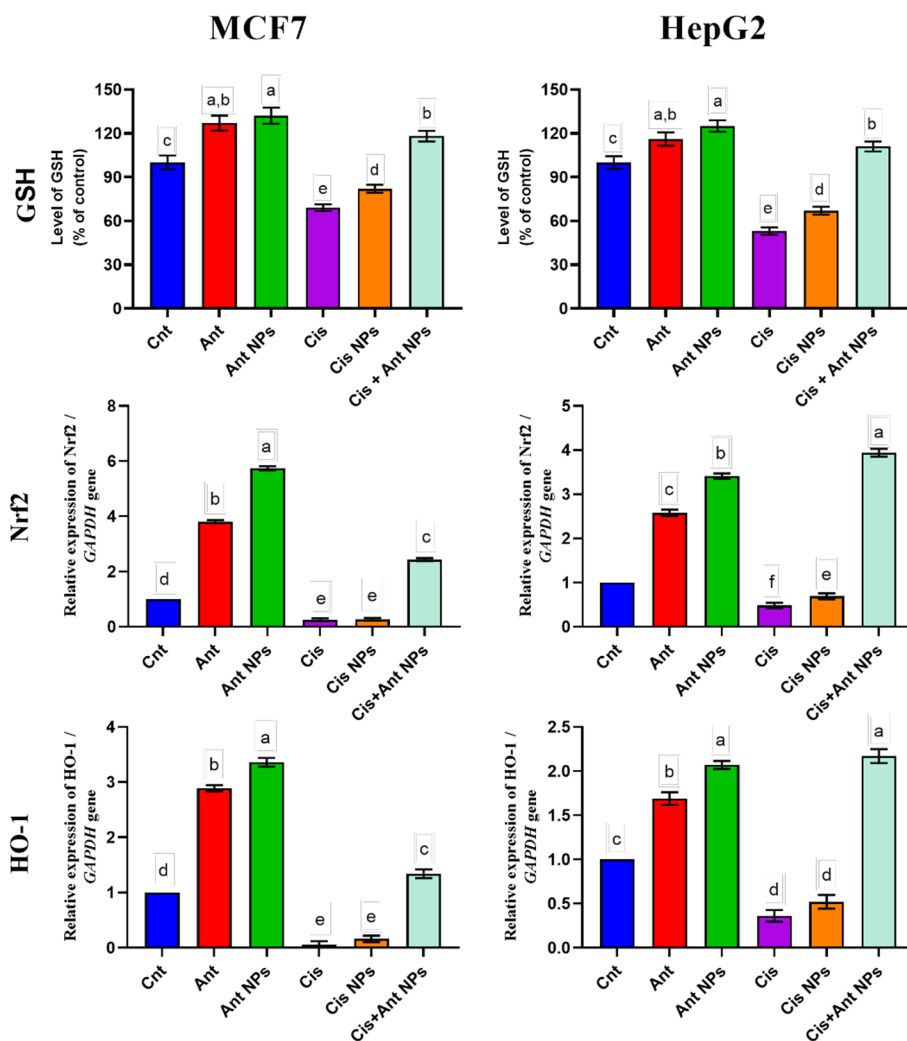


**Fig. 8** Effect of treatments on antioxidant status as revealed by determination of GSH levels and *Nrf2*, *HO-1* gene expression in MCF7 and HepG2 cells. Values are given as mean  $\pm$  SEM ( $n=3$ /group). Various letters [a (highest value)–e (lowest value)] denote significant differences at  $P < 0.05$ . All groups were compared to each other

drug resistance in cancer cells, reducing its effectiveness over time. In procedures like TACE, NP formulations could enhance the localized delivery of Cis, potentially increasing the drug’s efficacy while minimizing systemic side effects (Metkar et al. 2023). NPs can provide a controlled release of Cis, which may allow for sustained therapeutic concentrations over time, further improving the treatment’s impact (Costoya et al. 2022). On the other hand, Ants, particularly those derived from beetroot, can also prevent the viability of cancer cells (Li et al. 2021; Saber et al. 2023).

The MTT assay data revealed that treatment with Ant, Ant NPs, Cis, Cis NPs, and Cis + Ant NPs led to a significant dose-dependent cytotoxic effect on MCF7 and HepG2 with best effect for Cis. Unlike Cis, Ant and Ant NPs have demonstrated moderate-to-good cytotoxic activity towards HepG2 and MCF7 cells. On the other hand, when considering the drug concentration inside the capsule, nanocapsules in which the drug

concentration was around 10 times lower, demonstrated a little anti-cancer effect. This can explain why Ant NPs and/or Cis NPs showed lower cytotoxic potential (as revealed by higher  $IC_{50}$  values) on MCF7 and HepG2 cells than their non-capsulated forms (Ant and Cis). Given that the drug concentration in the NPs is 10 times lower than the free drug dose, the observed  $IC_{50}$  values for the nanoformulated drugs must be interpreted carefully. Ant NPs and Cis NPs demonstrated significantly higher  $IC_{50}$  values in MCF7 and HepG2 ( $57.12 \pm 1.78$ ,  $61.21 \pm 1.79$   $\mu\text{g/mL}$  for Ant NPs and  $21.26 \pm 1.33$  and  $18.18 \pm 1.26$   $\mu\text{g/mL}$  for Cis NPs, respectively). At first glance, this suggests a large reduction in cytotoxic potency but considering the 10 times lower concentration inside the NPs, these values are quite comparable. If the drug concentration inside the NPs were equivalent to the free drug, the adjusted  $IC_{50}$  values might approach 5.70, 6.12  $\mu\text{g/mL}$  for Ant NPs and 2.13, 1.82  $\mu\text{g/mL}$  for Cis NPs, respectively, which are lower than that of the free Ant and Cis  $IC_{50}$  values. The combined NPs formulation had  $IC_{50}$  values of  $20.59 \pm 1.31$   $\mu\text{g/mL}$  for MCF7 and  $33.30 \pm 1.52$   $\mu\text{g/mL}$  for HepG2. Adjusting for the lower drug concentrations, the effective  $IC_{50}$  values may approximate 2.06  $\mu\text{g/mL}$  for MCF7 and 1.33  $\mu\text{g/mL}$  for HepG2.

The cytotoxic impact of all treatments on the two cancer cell lines could be caused by apoptosis as evidenced by the morphological changes (chromatin condensation or disintegration and orange-colored nuclei of MCF7 and HepG2 stained with AO/EB), and the molecular changes (significant upregulation of the *Bax* gene and downregulation of the *Bcl2* gene). Cells treated with Cis+Ant NPs showed the greatest expression of *Bax* and the lowest expression of *Bcl2*, indicating maximum apoptosis and validating the impact of combined treatment with Ant and Cis. This also suggests that Ant's apoptosis-dependent cytotoxic potential is not specific to any one kind of cancer cell and is present in two different (liver and breast) cancer cell lines. Consistent with our findings, earlier in vitro research revealed that Ant and its primary metabolites triggered apoptosis in a large variety of cancers including liver HepG2, breast MDA-MB-453 (Li et al. 2016), leukemia U937 (Lee et al. 2009), prostate LNCaP, PC-3 (Reddivari et al. 2007), gastric adenocarcinoma (Shih et al. 2005), uterine carcinoma HeLa S3, colon CaCo-2 and HCT116 (Katsube et al. 2003; Lazzè et al. 2004), and leukemia HL60 (Katsube et al. 2003) cancer cells. The majority of these studies, including ours, indicated that the apoptosis-dependent cytotoxic effect of Ant correlated with the elevation of *Bax* and the lowering of *Bcl2* (Fang et al. 2018).

Since apoptosis is closely linked to cell cycle control, all treatments are being investigated for their ability to affect the cell cycle and the results showed that Ant, Cis, and their NPs could suppress MCF7 and HepG2 proliferation by inducing cell cycle arrest mainly in G2/M and S phases. This arrest could be due to the targeting of some important molecules involved in the cell cycle. In support, Ant showed significant anticancer effects by targeting molecules that regulate the cell cycle. Specifically, they inhibited cyclin D1 and cyclin E, which are crucial for progressing the cell cycle from the G1 to S phase, thereby preventing the proliferation of cancer cells. Studies have shown that Ant increases the expression of CDK inhibitors like p21 and p27, which further halt cell cycle progression, leading to cell cycle arrest in cancer cells (Dharmawansa et al. 2020; Lin et al. 2017). These effects make Ants promising candidates for cancer prevention and therapy (Hudlikar et al. 2020). We found that the arrest was prominent in cells treated

with Cis NPs and Cis + Ant NPs comparable to that of free Cis, suggesting that encapsulated Cis + Ant can be efficiently utilized as a substitute for Cis chemotherapy.

One major challenge in using Cis is the development of drug resistance by cancer cells. We also found elevated expression of drug resistance-related *MDR1* and *MAPK1* in MCF7 and HepG2 cells treated with Cis. To overcome this deleterious effect, researchers have explored using Cis NPs alone or combined with other anti-cancer drugs (Jeong et al. 2018; Joshy et al. 2022; Lin et al. 2017; Romani 2022). Similarly, we also reported a significantly reduced expression in the two genes following treatment with Ant NPs, Cis NPs, and Cis + Ant NPs. Cyanidin, a secondary Ant metabolite, has been shown to increase the effectiveness of chemotherapy in highly resistant breast cancer cells (MDA-MB-453). This effect is believed to be due to cyanidin's ability to inactivate signaling pathways (p-Akt and p-MAPK) that can promote cancer cell survival (Li et al. 2016).

Another significant disadvantage of using Cis for chemotherapy is that it induces oxidative stress, not just in cancer cells, but also in healthy cells throughout the body (Abass et al. 2024; Zraik and Heß-Busch 2021). In support, our results revealed that cancer cells treated with Cis and Cis NPs showed a considerable increase in oxidative stress as evidenced by reduced GSH levels and downregulation of the antioxidant-related *Nrf2* and *HO-1* genes. Similar Cis effects on cancer cells were reported by other researchers (Babaei et al. 2019; Hussain et al. 2021). In contrast, treatment with Ant, Ant NPs, and Cis + Ant NPs significantly increased GSH levels and upregulated the expression of the two antioxidant genes. These increases were not only greater than those observed in Cis and Cis NPs groups but also surpassed the levels seen in control cells. Similarly, *Nrf2* and *HO-1* activation in the endothelial cells are significantly influenced by Ant extracted from grape pomace (Herrera-Bravo et al. 2022). Because Ants can counteract the harmful effects of oxidative stress on cancer cells, they are being recognized for their possible anticancer benefits. For example, in a clinical trial with healthy people, red mixed berry juice rich in Ants helped protect their DNA from damage and boosted the antioxidant status as indicated by higher levels of GSH (Weisel et al. 2006). A different clinical trial showed that daily intake of fruits enriched with Ants was associated with a decrease in breast cancer recurrence, possibly due to its ability to suppress oxidative stress triggered by cancer cell (Butalla et al. 2012). Cis stimulates cancer cell death by augmenting reactive oxygen species (ROS) and diminishing antioxidant defenses, causing damage to healthy cells as well. In contrast, Ant, particularly in the form of nanoparticles (Ant NPs), greatly enhanced GSH levels, reinstating antioxidant defenses and mitigating oxidative stress (Fang et al. 2020). Cis NPs also showed a slightly higher antioxidant status than Cis, indicating the improvement of chemotherapy performance through encapsulation (Zhu et al. 2019). The combination of Cis + Ant NPs demonstrated encouraging outcomes, achieving a balance between efficient targeting of cancer cells and minimal effects on normal cells (Qi et al. 2017). Ant NPs may defend against damage caused by Cis while maintaining its anticancer effectiveness (Amararathna et al. 2022). This underscores the possibility of using natural antioxidants, such as Ant, in conjunction with chemotherapy encapsulation to improve treatment results and minimize adverse effects.

Metastasis and multi-organ dysfunction may be responsible for the majority of cancer-related deaths. Thus, a key advantage of powerful anticancer medications is their ability to prevent cancer cells from metastasis. In the present study, treatment with Ant, Cis,

and their NPs was found to effectively block the migration and metastasis of MCF7 and HepG2 cells. This effect was linked to a significant decrease in *MMP9*, a gene involved in metastasis, and a significant increase in *TIMP1*, a gene that suppresses metastasis. Again, the combination of Cis NPs with Ant NPs showed the strongest effect compared to treatment with either agent alone. These results agreed with previous studies which revealed that black rice-derived Ants can hinder the migration and metastasis of a large variety of breast and liver cancer cells, at least partly, by blocking *MMP2* and *MMP9* and by activating *TIMP1* (Chen et al. 2015; Hui et al. 2010). Moreover, the Ant secondary metabolites, malvidin 3-glucoside and delphinidin 3-glucoside (D3G), also inhibit colon cancer HCT-116 cells via the inactivation of *MMP2* and *MMP9* (Shin et al. 2011).

According to scientific research, effective cancer drugs have the ability to reduce inflammation and prevent the formation of new blood vessels. Our results showed inhibition of angiogenesis (as revealed by decreased *VEGF*) in all treated MCF7 and HepG2. These treatments also reduced inflammation (as marked by lower *TNF $\alpha$*  expression) except in Cis-treated cells. The best anti-angiogenic and anti-inflammatory effect was noticed in the Cis+Ant NPs treated cells. Our findings align with previous research, which suggests that Ants exert their anti-cancer effects by reducing levels of *TNF $\alpha$*  and *VEGF* (Lin et al. 2017; Pan et al. 2010). Ants extracted from cocoplum induced a cytotoxic effect on colorectal HT-29 cancer cells and this effect is mediated by the inhibition of *IL1 $\beta$* , *TNF $\alpha$* , *IL6*, and *NF $\kappa$ B* cytokines (Venancio et al. 2017). Berries-derived Ants exhibit promising anticancer properties by suppressing the activity of inflammatory signaling pathways (*MAPK*, *NF- $\kappa$ B*, *COX-2*, *TNF- $\alpha$* , *IL-6*, and *VEGF*), which promote inflammation and cancer cell growth (Huang et al. 2006; Pan et al. 2010).

There are some limitations of our study. While this study demonstrates promising results in cell lines, further in vivo studies using animal models are necessary to assess the efficacy and safety of this approach in a whole organism. The study mainly focused on gene expression changes associated with various anti-cancer effects. Additional protein detection methods, such as Western blotting (WB), would strengthen the findings by confirming protein level changes for key molecules. Another limitation of this study is the lack of functional assays, such as transwell migration and wound scratch assays, which would provide direct evidence of the effects on cell migration and invasion. Future studies should include these functional assays to corroborate our findings.

## Conclusions

Our study demonstrates the promising potential of combining anthocyanins with cisplatin-loaded chitosan nanoparticles for breast (MCF7) and liver (HepG2) cancer treatment. This novel approach appears to exert its anti-cancer effects through multiple mechanisms, including inducing apoptosis (high *Bax*, DNA fragmentation, and low *Bcl2*), cell cycle arrest (in G2/M, and S phases), and inhibition of drug resistance (low *MAPK1* and *MDR1*), metastasis (low *MMP9* and high *TIMP1*), oxidative stress (high *Nrf2* and *HO-1*), inflammation (low *TNF $\alpha$* ), and angiogenesis (low *VEGF*), as shown in Fig. 9. These findings provide encouraging evidence for the development of novel therapeutic strategies for breast and liver cancers by harnessing the synergistic effects of anthocyanins and cisplatin. Future research will pave the way for the

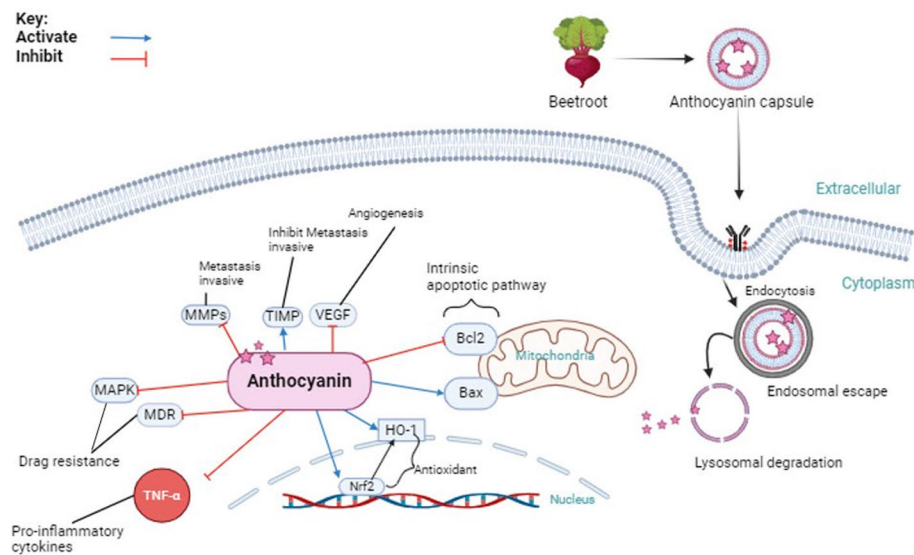


**Fig. 9** Main potential molecular mechanism of the antitumor effect of anthocyanin in vitro. This figure summarizes how anthocyanin encapsulation interferes with key cancer cell survival/death mechanisms, including proliferation, metastasis, angiogenesis, apoptosis regulation, antioxidant defenses, and inflammation. The end result is reduced cancer cell viability and improved sensitivity to treatments

safe and effective translation of this approach into clinical practice. This includes pre-clinical studies in animal models to assess the efficacy and safety of this approach. In addition, further investigation into the optimal dosing regimen and potential side effects of this combination therapy is crucial.

### Supplementary Information

The online version contains supplementary material available at <https://doi.org/10.1186/s12645-024-00297-9>.

Supplementary Material 1.

### Acknowledgements

Not applicable.

### Author contributions

N. H., R.A. and M.E. designed the experiment; M.A., D. A. and S.E. conducted the experiment; M.A., N. H. and M.E. analyzed the data; M.A., D. A. and S.E. wrote the first draft of the article; N. H., R.A. and M.E. revised the article; All authors reviewed the manuscript.

### Funding

Open access funding provided by The Science, Technology & Innovation Funding Authority (STDF) in cooperation with The Egyptian Knowledge Bank (EKB). No external funds were received.

### Availability of data and materials

No datasets were generated or analysed during the current study.

### Declarations

#### Ethics approval and consent to participate

Not applicable as the study was performed on purchased cell lines and no involvement of animals or humans samples.

#### Consent for publication

All the authors agree to the publication of this manuscript.

### Competing interests

The authors declare no competing interests.

Received: 15 July 2024 Accepted: 4 November 2024

Published online: 16 November 2024

### References

- Abass SA, Elgazar AA, El-kholy SS, El-Refaiy AI, Nawaya RA, Bhat MA, Farrag FA, Hamdi A, Balaha M, El-Magd MA (2024) Unraveling the nephroprotective potential of papaverine against cisplatin toxicity through mitigating oxidative stress and inflammation: insights from in silico, in vitro, and in vivo investigations. *Molecules*. <https://doi.org/10.3390/molecules29091927>
- Abdelkawy KS, El-Haggar SM, Ziada DH, Ebaid NF, El-Magd MA, Elbarbry FA (2020) The effect of genetic variations on ribavirin pharmacokinetics and treatment response in HCV-4 Egyptian patients receiving sofosbuvir/daclatasvir and ribavirin. *Biomed Pharmacother* 121:109657
- Ali R, Aouida M, Alhaj Sulaiman A, Madhusudan S, Ramotar D (2022) Can cisplatin therapy be improved? pathways that can be targeted. *Int J Mol Sci* 23:7241
- Al-Muftah M, Al-Ejeh F (2023) Cancer incidence and mortality estimates in Arab countries in 2018: a GLOBOCAN data analysis. *Cancer Epidemiol Biomark Prev* 32:1738–1746
- Amararathna M, Hoskin DW, Rupasinghe HPV (2022) Anthocyanin encapsulated nanoparticles as a pulmonary delivery system. *Oxid Med Cell Longev* 2022:1422929
- Anand U, Dey A, Chandel AKS, Sanyal R, Mishra A, Pandey DK, De Falco V, Upadhyay A, Kandimalla R, Chaudhary A, Dhanjal JK, Dewanjee S, Vallamkondu J, Pérez de la Lastra JM (2023) Cancer chemotherapy and beyond: current status, drug candidates, associated risks and progress in targeted therapeutics. *Genes Dis* 10:1367–1401
- Aramaki O, Takayama T, Moriguchi M, Sakamoto H, Yodono H, Kokudo N, Yamanaka N, Kawasaki S, Sasaki Y, Kubota K, Otsuji E, Tanaka S, Matsuyama Y, Fujii M (2021) Arterial chemoembolisation with cisplatin versus epirubicin for hepatocellular carcinoma (ACE 500 study): a multicentre, randomised controlled phase 2/3 trial. *Eur J Cancer* 157:373–382
- Attia AA, Salama AF, Eldiasty JG, Mosallam SAE, El-Naggar SA, El-Magd MA, Nasser HM, Elmetwalli A (2022) Amygdalin potentiates the anti-cancer effect of Sorafenib on Ehrlich ascites carcinoma and ameliorates the associated liver damage. *Sci Rep* 12:6494
- Awad MG, Ali RA, Abd El-Monem DD, El-Magd MA (2020) Graviola leaves extract enhances the anticancer effect of cisplatin on various cancer cell lines. *Mol Cell Toxicol*. <https://doi.org/10.1007/s13273-020-00092-8> 16:385–399
- Babaei F, Ebrahimi Shahmabadi H, Rajabi MR, Haddad Kashani H, Izadpanah F (2019) Evaluation of cisplatin efficacy on HepG2 and *E. coli* cells under acidic conditions. *Asian Pac J Cancer Prevent* 20:723–726
- Benchagra L, Berrougui H, Islam MO, Ramchoun M, Boulbaroud S, Hajjaji A, Fulop T, Ferretti G, Khalil A (2021) Antioxidant effect of Moroccan pomegranate (*Punica granatum* L. Sefri Variety) extracts rich in punicalagin against the oxidative stress process. *Foods* 10:2219
- Butalla AC, Crane TE, Patil B, Wertheim BC, Thompson P, Thomson CA (2012) Effects of a carrot juice intervention on plasma carotenoids, oxidative stress, and inflammation in overweight breast cancer survivors. *Nutr Cancer* 64:331–341
- Chen X-Y, Zhou J, Luo L-P, Han B, Li F, Chen J-Y, Zhu Y-F, Chen W, Yu X-P (2015) Black rice anthocyanins suppress metastasis of breast cancer cells by targeting RAS/RAF/MAPK pathway. *Biomed Res Int* 2015:414250
- Chen S, Wu Q, Li X, Li D, Mei N, Ning B, Puig M, Ren Z, Tolleson WH, Guo L (2021) Characterization of cytochrome P450s (CYP)-overexpressing HepG2 cells for assessing drug and chemical-induced liver toxicity. *J Environ Sci Health Part C Toxicol Carcinog* 39:68–86
- Costoya J, Surnar B, Kalathil AA, Kolishetti N, Dhar S (2022) Controlled release nanoplatforams for three commonly used chemotherapeutics. *Mol Aspects Med* 83:101043
- Dasari S, Tchounwou PB (2014) Cisplatin in cancer therapy: molecular mechanisms of action. *Eur J Pharmacol* 740:364–378
- Dharmawansa KVS, Hoskin DW, Rupasinghe HPV (2020) Chemopreventive effect of dietary anthocyanins against gastrointestinal cancers: a review of recent advances and perspectives. *Int J Mol Sci* 21:6555
- Duan X, He C, Kron SJ, Lin W (2016) Nanoparticle formulations of cisplatin for cancer therapy. *Wiley Interdiscip Rev Nanomed Nanobiotechnol* 8:776–791
- El-Magd MA, Khamis A, Nasr Eldeen SK, Ibrahim WM, Salama AF (2017) Trehalose enhances the antitumor potential of methotrexate against mice bearing Ehrlich ascites carcinoma. *Biomed Pharmacother* 92:870–878
- Elserafi MM, Zeeneldin AA, Abdelsalam IM, Nassar HR, Moneer MM, Buhoush WH (2018) First-line paclitaxel and cisplatin used sequentially or in combination in metastatic breast cancer: a phase II randomized study. *J Egypt Natl Canc Inst* 30:13–20
- Emran TB, Shahriar A, Mahmud AR, Rahman T, Abir MH, Siddiquee MF, Ahmed H, Rahman N, Nainu F, Wahyudin E, Mitra S, Dhama K, Habiballah MM, Haque S, Islam A, Hassan MM (2022) Multidrug resistance in cancer: understanding molecular mechanisms, immunoprevention and therapeutic approaches. *Front Oncol* 12:891652
- Falzone L, Salomone S, Libra M (2018) Evolution of cancer pharmacological treatments at the turn of the third millennium. *Front Pharmacol* 9:1300
- Fan H, Ji Y, Wang Y, Liu D, Wei T, Cao X, Yang M, Bai C, Wang Z (2022) Anthocyanins from *Lycium ruthenicum* murray inhibit HepG2 cells growth, metastasis and promote apoptosis and G2/M phase cycle arrest by activating the AMPK/mTOR autophagy pathway. *Evid-Based Complement Altern Med* 2022:9609596
- Fang Z, Hongfei Z, Bolin Z, Yanping J (2018) Blueberry anthocyanin induces apoptosis in HepG-2 cells and the mechanism of the process. *Eur Food Res Technol* 244:301–311

- Fang J-L, Luo Y, Yuan K, Guo Y, Jin S-H (2020) Preparation and evaluation of an encapsulated anthocyanin complex for enhancing the stability of anthocyanin. *LWT* 117:108543
- Forner A, Reig M, Bruix J (2018) Hepatocellular carcinoma. *Lancet* 391:1301–1314
- Ghaffari T, Hong JH, Asnaashari S, Farajnia S, Delazar A, Hamishehkar H, Kim KH (2021) Natural phytochemicals derived from gymnosperms in the prevention and treatment of cancers. *Int J Mol Sci* 22:6636
- Ghasemi M, Liang S, Luu QM, Kempson I (2023) The MTT assay: a method for error minimization and interpretation in measuring cytotoxicity and estimating cell viability. In: Friedrich O, Gilbert DF (eds) *Cell viability assays: methods and protocols*. Springer, New York, pp 15–33
- Ghiman R, Nistor M, Focșan M, Pinteș A, Aștilean S, Rugina D (2021) Fluorescent polyelectrolyte system to track anthocyanins delivery inside melanoma cells. *Nanomaterials* 11:782
- Gonçalves AC, Falcão A, Alves G, Lopes JA, Silva LR (2022) Employ of anthocyanins in nanocarriers for nano delivery: in vitro and in vivo experimental approaches for chronic diseases. *Pharmaceutics* 14:2272
- Guiné R, Gonçalves F, Lerat C, Idrissi T, Rodrigo E, Correia P, Gonçalves JC (2018) Extraction of phenolic compounds with antioxidant activity from beetroot (*Beta vulgaris* L.). *Curr Nutr Food Sci* 14:350–357
- Guiné R, Mendes M, Gonçalves F (2019) Optimization of bioactive compound's extraction conditions from beetroot by means of artificial neural networks (ANN). *Agric Eng Int CIGR e-J* 21:216–223
- Hamaya S, Oura K, Morishita A, Masaki T (2023) Cisplatin in liver cancer therapy. *Int J Mol Sci* 24:10858
- Hanafy NAN (2021) Starch based hydrogel NPs loaded by anthocyanins might treat glycogen storage at cardiomyopathy in animal fibrotic model. *Int J Biol Macromol* 183:171–181
- Hanafy NAN, Salim EI, Mahfouz ME, Eltonouby EA, Hamed IH (2023) Fabrication and characterization of bee pollen extract nanoparticles: their potential in combination therapy against human A549 lung cancer cells. *Food Hydrocoll Health* 3:100110
- He Q, Shi J (2014) MSN anti-cancer nanomedicines: chemotherapy enhancement, overcoming of drug resistance, and metastasis inhibition. *Adv Mater* 26:391–411
- Herrera-Bravo J, Beltrán JF, Huard N, Saavedra K, Saavedra N, Alvear M, Lanas F, Salazar LA (2022) Anthocyanins found in pinot noir waste induce target genes related to the Nrf2 signalling in endothelial cells. *Antioxidants* 11:1239
- Huang C, Li J, Song L, Zhang D, Tong Q, Ding M, Bowman L, Aziz R, Stoner GD (2006) Black raspberry extracts inhibit benzo (a) pyrene diol-epoxide-induced activator protein 1 activation and VEGF transcription by targeting the phosphatidylinositol 3-kinase/Akt pathway. *Can Res* 66:581–587
- Hudlikar R, Wu R, Cheng D, Kuo DH-C, Wang L, Peter R, Yin R, Li S, Kong A-N (2020) Anthocyanins and cancer prevention. In: Pezzuto JM, Vang O (eds) *Natural products for cancer chemoprevention: single compounds and combinations*. Springer International Publishing, Cham, pp 351–373
- Hui C, Bin Y, Xiaoping Y, Long Y, Chunye C, Mantian M, Wenhua L (2010) Anticancer activities of an anthocyanin-rich extract from black rice against breast cancer cells in vitro and in vivo. *Nutr Cancer* 62:1128–1136
- Hussain Y, Islam L, Khan H, Filosa R, Aschner M, Javed S (2021) Curcumin-cisplatin chemotherapy: a novel strategy in promoting chemotherapy efficacy and reducing side effects. *Phytother Res* 35:6514–6529
- Jeong Y-H, Shin H-W, Kwon J-Y, Lee S-M (2018) Cisplatin-encapsulated polymeric nanoparticles with molecular geometry-regulated colloidal properties and controlled drug release. *ACS Appl Mater Interfaces* 10:23617–23629
- Jeyaram S, Geethakrishnan T (2020) Vibrational spectroscopic, linear and nonlinear optical characteristics of Anthocyanin extracted from blueberry. *Results Opt* 1:100010
- Joshi KS, Hasan A, Augustine R, Alex S, Zahid A, Dalvi Y, Mraiche F, Thomas S, Kalarikkal N, Chi H (2022) Cisplatin encapsulated nanoparticles from polymer blends for anti-cancer drug delivery. *New J Chem* 46:5819
- Kari S, Subramanian K, Altomonte IA, Murugesan A, Yli-Harja O, Kandhavelu M (2022) Programmed cell death detection methods: a systematic review and a categorical comparison. *Apoptosis* 27:482–508
- Katsube N, Iwashita K, Tsushida T, Yamaki K, Kobori M (2003) Induction of apoptosis in cancer cells by bilberry (*Vaccinium myrtillus*) and the anthocyanins. *J Agric Food Chem* 51:68–75
- Lazzè MC, Savio M, Pizzala R, Cazzalini O, Perucca P, Scovassi AI, Stivala LA, Bianchi L (2004) Anthocyanins induce cell cycle perturbations and apoptosis in different human cell lines. *Carcinogenesis* 25:1427–1433
- Lee SH, Park SM, Park SM, Park JH, Shin DY, Kim GY, Ryu CH, Shin SC, Jung JM, Kang HS, Lee WS, Choi YH (2009) Induction of apoptosis in human leukemia U937 cells by anthocyanins through down-regulation of Bcl-2 and activation of caspases. *Int J Oncol* 34:1077–1083
- Li X, Xu J, Tang X, Liu Y, Yu X, Wang Z, Liu W (2016) Anthocyanins inhibit trastuzumab-resistant breast cancer in vitro and in vivo. *Mol Med Rep* 13:4007–4013
- Li X, Chen L, Gao Y, Zhang Q, Chang AK, Yang Z, Bi X (2021) Black raspberry anthocyanins increased the antiproliferative effects of 5-Fluorouracil and Celecoxib in colorectal cancer cells and mouse model. *J Funct Foods* 87:104801
- Lin BW, Gong CC, Song HF, Cui YY (2017) Effects of anthocyanins on the prevention and treatment of cancer. *Br J Pharmacol* 174:1226–1243
- Lin SR, Chang CH, Hsu CF, Tsai MJ, Cheng H, Leong MK, Sung PJ, Chen JC, Weng CF (2020) Natural compounds as potential adjuvants to cancer therapy: preclinical evidence. *Br J Pharmacol* 177:1409–1423
- Łukasiewicz S, Czeczeliński M, Forma A, Baj J, Sitarz R, Stanisławek A (2021) Breast cancer-epidemiology, risk factors, classification, prognostic markers, and current treatment strategies-an updated review. *Cancers* 13:4287
- Lv L, Luo H, Yu L, Tong W, Jiang Y, Li G, Tong G, Li Y, Liu C (2022) Identification and characterization of cell lines HepG2, Hep3B217 and SNU387 as models for porcine epidemic diarrhea coronavirus infection. *Viruses* 14:2754
- Masoud V, Pagès G (2017) Targeted therapies in breast cancer: new challenges to fight against resistance. *World J Clin Oncol* 8:120–134
- Mazalovska M, Kouokam JC (2020) Plant-derived lectins as potential cancer therapeutics and diagnostic tools. *Biomed Res Int* 2020:1631394
- Metkar SP, Fernandes G, Navti PD, Nikam AN, Kudarha R, Dhas N, Seetharam RN, Santhosh KV, Rao BSS, Mutalik S (2023) Nanoparticle drug delivery systems in hepatocellular carcinoma: a focus on targeting strategies and therapeutic applications. *OpenNano* 12:100159

- Obidiro O, Battogtokh G, Akala EO (2023) Triple negative breast cancer treatment options and limitations: future outlook. *Pharmaceutics* 15:1796
- Pan M-H, Lai C-S, Ho C-T (2010) Anti-inflammatory activity of natural dietary flavonoids. *Food Funct* 1:15–31
- Parveen Zia MS, Sneha S (2021) Extraction of natural colour from beet root (*Beta vulgaris*) its phytochemical analysis and antibacterial activity. *EAS J Nutr Food Sci* 3:6
- Qi Z-L, Wang Z, Li W, Hou J-G, Liu Y, Li X-D, Li H-P, Wang Y-P (2017) Nephroprotective effects of anthocyanin from the fruits of (GFA) on cisplatin-induced acute kidney injury in mice. *Phytother Res* 31:1400–1409
- Rabelo ACS, Guerreiro CA, Shinzato VI, Ong TP, Noratto G (2023) Anthocyanins reduce cell invasion and migration through Akt/mTOR downregulation and apoptosis activation in triple-negative breast cancer cells: a systematic review and meta-analysis. *Cancers* 15:2300
- Reddivari L, Vanamala J, Chintharlapalli S, Safe SH, Miller JC Jr. (2007) Anthocyanin fraction from potato extracts is cytotoxic to prostate cancer cells through activation of caspase-dependent and caspase-independent pathways. *Carcinogenesis* 28:2227–2235
- Romani AMP (2022) Cisplatin in cancer treatment. *Biochem Pharmacol* 206:115323
- Saber A, Abedimanesh N, Somi M-H, Khosroushahi AY, Moradi S (2023) Anticancer properties of red beetroot hydro-alcoholic extract and its main constituent; betanin on colorectal cancer cell lines. *BMC Complement Med Ther* 23:246
- Salehi B, Sharif-Rad J, Cappellini F, Reiner Ž, Zorzan D, Imran M, Sener B, Kilic M, El-Shazly M, Fahmy NM, Al-Sayed E, Martorell M, Tonelli C, Petroni K, Docea AO, Calina D, Maroyi A (2020) The therapeutic potential of anthocyanins: current approaches based on their molecular mechanism of action. *Front Pharmacol* 11:1300
- Selim NM, Elgazar AA, Abdel-Hamid NM, El-Magd MRA, Yasri A, Hefnawy HME, Sobeh M (2019) Chrysophanol, hesperidin and curcumin modulate the gene expression of pro-inflammatory mediators induced by LPS in Hep G2: in silico and molecular studies. *Antioxidants* 8:371
- Shen Y, Zhang N, Tian J, Xin G, Liu L, Sun X, Li B (2022) Advanced approaches for improving bioavailability and controlled release of anthocyanins. *J Control Release* 341:285–299
- Shih P-H, Yeh C-T, Yen G-C (2005) Effects of anthocyanidin on the inhibition of proliferation and induction of apoptosis in human gastric adenocarcinoma cells. *Food Chem Toxicol* 43:1557–1566
- Shin DY, Lu JN, Kim G-Y, Jung JM, Kang HS, Lee WS, Choi YH (2011) Anti-invasive activities of anthocyanins through modulation of tight junctions and suppression of matrix metalloproteinase activities in HCT-116 human colon carcinoma cells. *Oncol Rep* 25:567–572
- Siegel RL, Miller KD, Jemal A (2020) Cancer statistics, 2020. *CA Cancer J Clin* 70:7–30
- Stavenga DG, Leertouwer HL, Dudek B, van der Kooij CJ (2020) Coloration of flowers by flavonoids and consequences of pH dependent absorption. *Front Plant Sci* 11:600124
- Sultan MH, Moni SS, Madkhali OA, Bakkari MA, Alshahrani S, Alqahtani SS, Alhakamy NA, Mohan S, Ghazwani M, Bukhari HA, Almohari Y, Salawi A, Alshamrani M (2022) Characterization of cisplatin-loaded chitosan nanoparticles and rituximab-linked surfaces as target-specific injectable nano-formulations for combating cancer. *Sci Rep* 12:468
- Tawfic AA, Ibrahim HM, Mohammed-Geba K, El-Magd MA (2024) Chitosan nanoparticles, camel milk exosomes and/or Sorafenib induce apoptosis, inhibit tumor cells migration and angiogenesis and ameliorate the associated liver damage in Ehrlich ascites carcinoma-bearing mice. *Beni-Suef Univ J Basic Appl Sci* 13:74
- Thibado SP, Thornthwaite JT, Ballard TK, Goodman BT (2018) Anticancer effects of Bilberry anthocyanins compared with NutraNanoSphere encapsulated Bilberry anthocyanins. *Mol Clin Oncol* 8:330–335
- Tsai MC, Chen CC, Tseng TH, Chang YC, Lin YJ, Tsai IN, Wang CC, Wang CJ (2023) Hibiscus anthocyanins extracts induce apoptosis by activating AMP-activated protein kinase in human colorectal cancer cells. *Nutrients* 15:3972
- Venancio VP, Cipriano PA, Kim H, Antunes LM, Talcott ST, Mertens-Talcott SU (2017) Cocoplum (*Chrysobalanus icaco* L.) anthocyanins exert anti-inflammatory activity in human colon cancer and non-malignant colon cells. *Food Funct* 8:307–314
- Weisel T, Baum M, Eisenbrand G, Dietrich H, Will F, Stockis JP, Kulling S, Rüfer C, Johannes C, Janzowski C (2006) An anthocyanin/polyphenolic-rich fruit juice reduces oxidative DNA damage and increases glutathione level in healthy probands. *Biotechnol J Healthc Nutr Technol* 1:388–397
- Yang B, Dong Y, Wang F, Zhang Y (2020) Nanoformulations to enhance the bioavailability and physiological functions of polyphenols. *Molecules* 25:4613
- Zbiral B, Weber A, Vivanco MD, Toca-Herrera JL (2023) Characterization of breast cancer aggressiveness by cell mechanics. *Int J Mol Sci* 24:12208
- Zedan AMG, Sakran MI, Bahattab O, Hawsawi YM, Al-Amer O, Oyouni AAA, Nasr Eldeen SK, El-Magd MA (2021) Oriental hornet (*Vespa orientalis*) larval extracts induce antiproliferative, antioxidant, anti-inflammatory, and anti-migratory effects on MCF7 cells. *Molecules* 26:3303. <https://doi.org/10.3390/molecules26113303>
- Zhang C, Xu C, Gao X, Yao Q (2022) Platinum-based drugs for cancer therapy and anti-tumor strategies. *Theranostics* 12:2115–2132
- Zhu L-J, Gu L-S, Shi T-Y, Zhang X-Y, Sun B-W (2019) Enhanced treatment effect of nanoparticles containing cisplatin and a GSH-reactive probe compound. *Mater Sci Eng C* 96:635–641
- Zraik IM, Heß-Busch Y (2021) Management of chemotherapy side effects and their long-term sequelae. *Der Urologe Ausg A* 60:862–871

## Publisher's Note

Springer Nature remains neutral with regard to jurisdictional claims in published maps and institutional affiliations.